Düzce University
Journal of Science & Technology

Research Article

Energy And Exergy Analysis For A New Models With Gradual Expansion Combined With Multiple Power Generation Systems

Ahmet ELBİR [a,*]

[a] *Suleyman Demirel University, YEKARUM, Isparta, TURKEY*
** Corresponding author's e-mail address:ahmetelbir@sdu.edu.tr*
DOI: 10.29130/dubited.1460109

ABSTRACT

Our utilization of waste heat sources, combined with multiple power generation systems and systems featuring gradual expansion, constitutes a crucial domain in terms of energy and exergy analysis. Within these systems, the utilization of energies derived from various power sources reveals the availability of system components, highlighting the importance of meticulous analysis during design and operation to mitigate energy and exergy losses. Energy and exergy analysis stands as a pivotal method employed throughout the design, operation, and maintenance phases of these systems. This study initiates with the commencement of the combustion chamber temperature and turbine output temperature of a UGT-25000 gas turbine, followed by the development of the system through gradual expansion processes. A comprehensive thermodynamic analysis of the integrated power generation system was conducted, encompassing heat transitions across the H_2O Rankine cycle, R113 ORC cycle, S-CO_2 cycle, electrolyzer, and NH_3H_2O absorption cycle along with successive sub-cycles. Additionally, energy extraction from turbines was facilitated through the gradual expansion of the air-Brayton, R113-ORC, H_2O-Rankine, and S-CO_2 cycles. The resulting net powers are as follows: 0.0034 kg/s of hydrogen produced with the electrolyzer from the Air Brayton cycle, 34.314 kW; H_2O Rankine cycle, 1.828 kW; R113 ORC, 681 kW; NH_3H_2O absorption cycle, 2.985 kW; and S-CO_2 cycle, 1.720 kW. The energy efficiency of the multi-integrated system is calculated to be 66.35%, with an exergy efficiency of 35%.

Keywords: *Energy analysis 1, Exergy analysis 2, Brayton cycle 3, Rankine cycle 4, Organic rankine cycle 5, Absorption cycle 6, Electolyzer 7*

Kademeli Genişlemeli Çoklu Güç Üretim Sistemleri İle Birlikte Yeni Modeller İçin Enerji ve Ekserji Analizi

ÖZET

Atık ısıl kaynakların kullanımı, birden fazla güç üretim sistemi ve kademeli genişleme özelliklerine sahip sistemlerle birleştirilerek, enerji ve ekserji analizi açısından kritik bir alan oluşturur. Bu sistemler içinde, çeşitli güç kaynaklarından elde edilen enerjilerin kullanımı, sistem bileşenlerinin kullanılabilirliğini ortaya çıkararak, tasarım ve işletme sırasında enerji ve ekserji kayıplarını azaltmak için titiz bir analizin önemini vurgular. Enerji ve ekserji analizi, bu sistemlerin tasarımı, işletilmesi ve

bakım aşamaları boyunca kullanılan temel bir yöntemdir. Bu çalışma, bir UGT-25000 gaz türbininin yanma odası sıcaklığı ve türbin çıkış sıcaklığı ile başlar ve ardından sistem, kademeli genişleme

Received: 27/03/2024, Revised: 2606/2024, Accepted: 02/07/2024

süreçleriyle geliştirilir. Entegre güç üretim sisteminin kapsamlı termodinamik analizi yapılmış olup, H_2O Rankine çevrimi, R113 ORC çevrimi, S-CO_2 çevrimi, elektrolizer ve NH_3H_2O emilim çevrimi ile ardışık alt çevrimler arasındaki ısı geçişlerini içerir. Ayrıca, türbünlardan enerji çıkarılması, hava-Brayton, R113-ORC, H_2O-Rankine ve S-CO_2 çevrimlerinin kademeli genişlemesi ile kolaylaştırılmıştır. Elde edilen net güçler aşağıdaki gibidir: Elektrolizerden Air Brayton çevrimiyle üretilen hidrojen miktarı 0.0034 kg/s, 34.314 kW; H_2O Rankine çevrimi, 1.828 kW; R113 ORC, 681 kW; NH_3H_2O emilim çevrimi, 2.985 kW; ve S-CO_2 çevrimi, 1.720 kW. Çoklu entegre sistemimizin enerji verimliliği %66.35 olarak hesaplanmış olup, ekserji verimliliği %35'tir.

Anahtar Kelimeler: *Enerji analizi 1, Ekserji analizi 2, Brayton çevrimi 3, Rankine çevrimi 4, Organik Rankine çevrimi 5, Emilim çevrimi 6, Elektrolizör 7*

I. INTRODUCTION

Global climate change is sounding an alarm, indicating the urgent need to transition away from fossil resources. The primary solution to address the demand for fossil fuels involves the development of integrated power generation systems that incorporate renewable energy sources and effectively utilize waste heat. Some systems possess significant energy value within their waste heat, and when these waste temperatures are appropriately harnessed, it not only reduces energy consumption but also enhances energy efficiency in overall process performance. The concept of energy efficiency is determined by the principle of entropy, representing disorder, and introduces the calculation of exergy. Exergy is a critical concept that reflects the quality of the resources utilized. Exergy losses are directly proportional to the entropy produced by the system. The mitigation of these losses or the identification of losses is achieved through the application of thermodynamic concepts. In this context, the energy analysis and exergy analysis of integrated systems derived from waste heat sources or renewable energy sources has recently gained significant importance.

Some studies in the literature: Mohammadi et al., introduced an innovative triple power cycle that harnesses waste heat derived from a gas turbine cycle. The researchers conducted thermodynamic analyses on the system, incorporating a S-CO_2 recompression cycle and a regenerative ORC [1]. Ran et al., endeavored to enhance the utilization of waste heat generated by a solid oxide fuel cell (SOFC). They introduced a novel multigenerational energy system and conducted a comprehensive thermodynamic analysis. The system comprises a SOFC, a micro gas turbine (MGT), a supercritical carbon dioxide (S-CO_2) Brayton cycle, and a lithium bromide absorption refrigerator [2]. Khan et al., made thermodynamic and exergo-environmental calculations of the performance of the multi-production system based on solar energy based on PCM (phase change material). solar tower with system helio, combined cycle (top Brayton cycle, bottom part Rankine cycle with reheating and regeneration processes), single-acting Lithium-Bromide/water intake chillergroup, heat pump, water-based They analyzed my system design, which consisted of a thermal energy storage system and an electrolyzer [3]. Khani et al., has designed and thermodynamically analyzed ORC into a solar-powered multi-generation system that integrates CO_2. In addition, the integrated system made calculations to meet the power, fresh water and carbon needs of a greenhouse [4]. Peng et al., conceptualized and performed thermodynamic analyses for a combined power and heat cogeneration system, incorporating a plasma gasifier, SOFC, gas turbine (GT), and a S-CO_2 cycle [5]. Khosravi., is to design an Organic Rankine Cycle based on geothermal energy that can be used for electricity generation, heating, cooling and decoding. It also envisaged its use for the production of hydrogen by means of electrolytes. In addition, it is aimed to recover the waste heat in the cycle, to drive the absorbable heat pump unit and to obtain heating, cooling and drying in this way [6]. Panahirad, orchestrated a comprehensive energy system encompassing a biomass-sourced combustion chamber (CC), a single-acting absorption cooling system (SEACS), an air conditioning unit (AC), a reheating vapor Rankine cycle (RSRC), an organic Rankine cycle (ORC), and an electrolyzer, conducting thorough thermodynamic calculations [7]. Zhang et al., devised an innovative hybrid system integrating compressed air energy storage (CAES) with

SOFC-GT. In this integrated system, the absence of power consumption during the air compressor's discharge process led to increased energy efficiency compared to traditional SOFC-GT configurations. Furthermore, they employed a Rankine steam cycle (RSC) to recover waste heat from the exhaust of the SOFC-GT [8]. Hai et al., expanded upon an existing solar-powered system by incorporating two power cycles, a thermoelectric generator, a hydrogen production unit, and absorption coolant subsystems. The study included analyses of energy, exergy, economic performance, and environmental impact of the system [9]. Wu et al., combined with the waste heat recovery (WHR) strategy, said that the efficiency of the system energy conversion could be further increased [10]. Qin et al., have conceptualized a novel combined cycle, comprising a supercritical CO_2 recompression Brayton cycle and a transcritical CO_2 cycle. They conducted a thermodynamic analysis of the cooling cycle to efficiently recover waste heat from a marine turbine for both power generation and cooling purposes [11]. Atif et al., designed a Combined Cooling, Heating, and Power (CCHP) system using S-CO_2. Their cycle involved integrating a Brayton cycle with a transcritical ejector cooling cycle through the addition of an extraction turbine, and a thorough thermodynamic analysis was performed [12]. Elbir et al., conducted analyses on both single and double-stage S-CO_2 Brayton cycles, incorporating intermediate heat exchangers operating within the same temperature range [13]. Gogoi et al., introduced a concept for a Combined Cycle Power Plant (CCPP) that integrates a gas turbine (GT) cycle, a regenerative steam turbine (ST) cycle, and a recuperative regenerative organic Rankine cycle (RR-ORC). The heat recovery steam generator (HRSG) efficiently utilized the GT cycle's exhaust gas to drive the ST cycle, while the remaining heat from the GT exhaust gas was effectively employed to power the RR-ORC through a heat recovery vapor generator (HRVG). The proposed CCPP showcased notable energy efficiency, reaching 44.79%, along with an exergy efficiency of 40.89% [14]. Bamisile et al., conceptualized, modeled, and analyzed two novel CO_2-based setups: the High-Temperature Geothermal Multi-Energy System (HTGMES) and the Low-Temperature Geothermal Multi-Energy System (LTGMES). These configurations were specifically designed to produce electricity, provide cooling/refrigeration, support space heating, generate hydrogen, and supply hot water. The determined steady-state overall energetic and exergetic efficiencies were 44.22% and 33.5% for HTGMES, and 45.40% and 32.9% for LTGMES, respectively [15]. Elmaihy et al., performed computational assessments on the energy and exergy aspects of harnessing waste heat from an automobile engine's cooling water via an Organic Rankine Cycle (ORC). The ORC, utilizing R245fa and R123 as working fluids, demonstrated peak thermal efficiencies of 7.76% and 7.49%, respectively [16]. Manesh et al., presented a comprehensive framework comprising a Brayton cycle, supercritical carbon dioxide (S-CO_2) cycle, organic Rankine cycle (ORC), and a polymer electrolyte membrane (PEM) electrolyzer. The integrated Brayton cycle system effectively captured exhaust heat, with seamless integration of S-CO_2 and ORC cycles utilizing this thermal resource. The combined energy and exergy efficiencies were documented at 40.95% and 39.49%, respectively [17]. Bamisile et al., presented a novel concentrated solar photovoltaic/thermal system hybridized with a wind turbine, creating a CO_2-based geothermal micro-multi-energy system. This proposed energy system, designed for electricity, cooling, space heating, hydrogen, and hot water generation, showcased overall energetic and exergetic efficiencies of2 48.61% and 88.31%, with the potential to increase to 51.76% and 95.08% through optimization based on system exergy efficiency [18]. Ding et al., assessed a comprehensive multi-energy configuration based on solar and geothermal energies, involving the Kalina (KC), ORC, cooling, water electrolysis, and thermoelectric (TEG) cycles. The system achieved an exergetic efficiency of 35.9% [19]. Cao et al., demonstrated the efficient recovery of waste heat from a hybrid solar-biomass heat source by employing a combined system of regenerative gas turbine cycle (GTC) and recompression S-CO_2 Brayton cycle (SCBC). The recovered waste heat was harnessed through diverse subsystems, including a thermoelectric generator, LiBr-H_2O absorption refrigerator system, heat recovery steam generator, and a proton exchange membrane electrolyzer. This integrated approach yielded an exergy efficiency of 43% and an energy efficiency of 62.2% [20].

Despite these advancements, there remains a critical need for further research to explore more effective integration strategies and enhance the overall efficiency of energy conversion systems. This study aims to fill this gap by proposing gradual expansion processes to enhance the efficiency of the UGT-25000 gas turbine. This novel approach seeks to achieve higher energy and exergy efficiencies through a comprehensive analysis of an integrated power generation system. The proposed system encompasses

various energy conversion technologies such as the H_2O Rankine cycle, R113 ORC cycle, S-CO_2 cycle, electrolyzer, and NH_3H_2O absorption cycle.

This study's originality lies in its holistic approach to integrating multiple energy conversion systems and its focus on the UGT-25000 gas turbine. By addressing these systems' combined energy and exergy analyses, this research provides a new perspective on optimizing energy conversion technologies and contributes significantly to the literature. The proposed methodologies and insights can pave the way for more efficient and sustainable power generation systems, thus contributing to the global effort to combat climate change.

II. MATERIALS AND METHODS

A. SYSTEM DESCRİPTİON

The integrated system providing multiple energy production is given in figure 1.

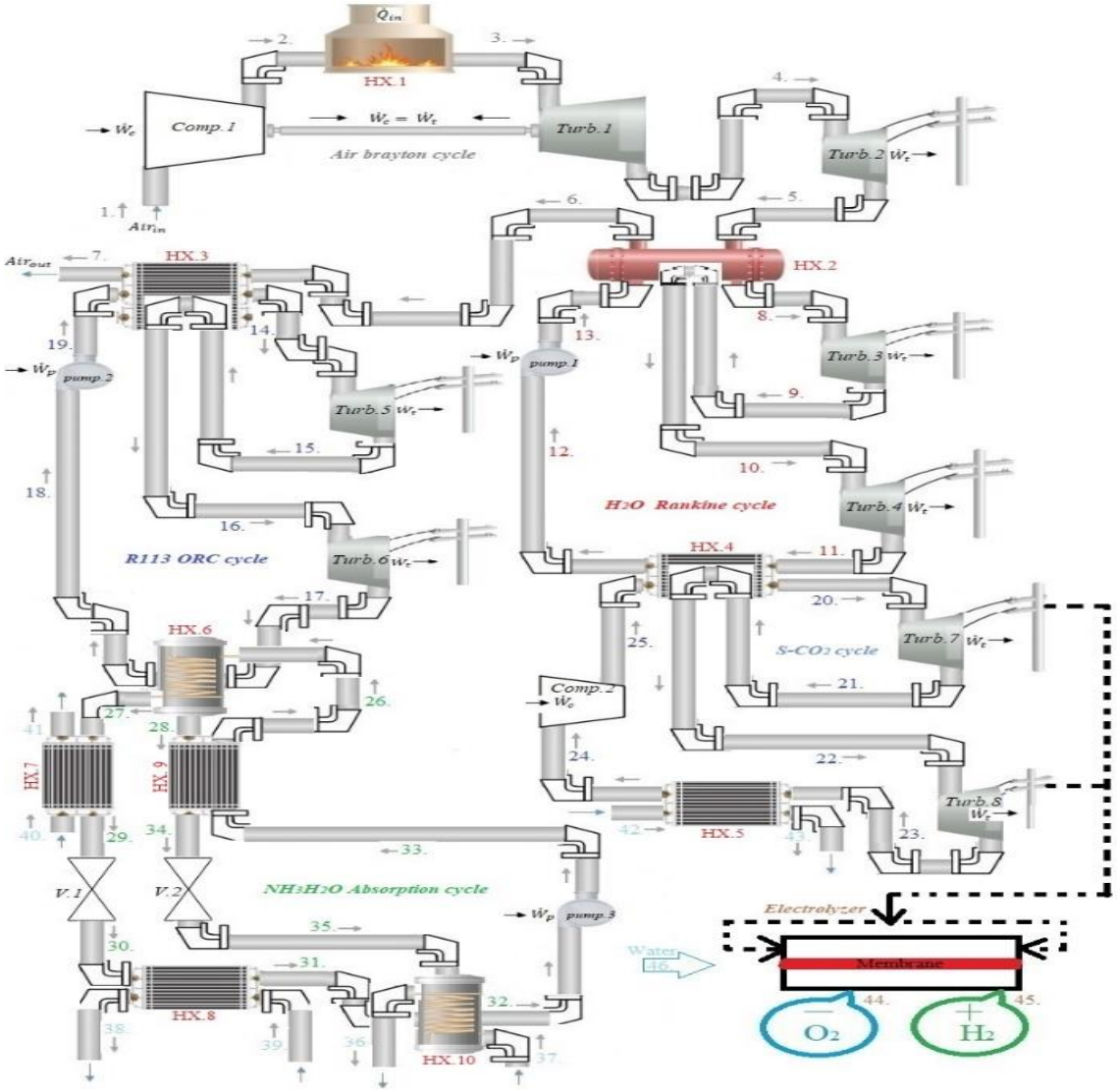

Figure 1. *Integrated system for multiple energy generation*

Air brayton cycle, The air entering in the 1st case exits the compressor in the 2nd case with the temperature and pressure increased. Then, with the heat received from the 1st heat exchanger (or

renewable energy source) from the heat source, the hot air that exits the temperature in the 3rd state with increased temperature passes through the turbine and provides electricity production. In the 4th case, the hot air coming out of the 1st turbine by falling by 1/4 passes through the 2nd turbine again and comes out in the 5th state with the pressure decreasing the atmosphere and the temperature decreased. The hot air in the 5th case passes through the 2nd heat exchanger and 3rd heat exchangers and transfers the heat to the lower cycles and the brayton cycle process ends.

H_2O rankine cycle, The 2nd heat exchanger sends the heat it receives to the 3rd turbine in the 8th state. In the 9th case, the heat generated is increased again and the temperature is increased again to the 2nd heat exchanger. The fluid that comes out at the 10th stage enters the 4th turbine and power generation is provided again. The heat of the fluid output in the 11th state is transferred to the 4th heat exchanger. The pressure of the fluid in the 12th state is increased with the 1st pump and the Rankine cevolution is completed.

R113 ORC, The fluid in its 14th state from the 3rd heat exchanger passes into the 5th tube. In the 15th case, it exits the turbine and re-enters the 3rd heat exchanger. In the 16th case, the fluid with increased temperature enters the 6th turbine and produces energy again. Then, the fluid in the 17th state transfers the heat to the NH_3H_2O absorption cooling cycle, which is a sub-cycle, with the 6th heat exchanger. In the 18th case, the fluid from the 6th heat exchanger passes to the 2nd pump to increase the pressure and in the 19th state the ORC is completed.

S-CO_2 cycle, With the heat received from the 4th heat exchanger, the fluid that exits in the 20th state exits from the 7th turbine in the 21st state and the temperature is increased again in the 4th heat exchanger. In the 22nd case, the fluid with increased temperature enters the 8th turbine and power production is provided again. The temperature of the fluid is reduced by throwing the temperature from the 5th heat exchanger into the water. The fluid in the 42nd state, whose temperature decreases, enters the 2nd compressor and completes the cycle by increasing the temperature and pressure.

Electolyzer, After the total power of the 7th turbine and the 8th turbine is met by the power of the 2nd compressor, the remaining power is transferred to the electrolyz. H_2O entering in case 46 passes through the electrolyzer and outputs O_2 in case 44 and H_2 in case 45.

NH_3H_2O Absorption cycle, 6. The heat received from the heat exchanger is transferred to the condenser in the 27th state after separation from the rich melt in the 27th state. 7.After the heat is lowered in the heat exchanger, the cooling melt passes through the 1st valve and 8. The heat exchanger passes into the evaporator at low temperature. In the 31st case, the 8th hea texchanger (evapoartor) exits fluid enters the absorber. Also 6.28. from heat exchanger. The fluid in the state passes through the 9th heat exchanger and passes through the 34th state The fluid passing through the 2nd valve enters the 10th heat exchanger (absorber) in the 35th case in order to reduce the pressure of the weak melt. In the 32nd case, the fluid from the 10th heat exchanger is sent to the 6th heat exchanger with the 3rd pump and the cycle is completed.

When performing a thermodynamic analysis of the multi-energy production system of the Tas bee, the following assumptions were taken into account:

- System performance is assumed to be stable and regular.
- Pure substance is used in the system.
- The compression in compressors is adiabatic.
- The heat entering and exiting the heat exchangers is equal to each other.
- Pressure drops in the system components and pipeline and the heat transfer process are alsoneglected.
- Opposite-flow heat exchangers were used in heat source heat exchangers, and heat losses were neglected.

- The dead state of the fluids circulating in the system (air, CO_2, water, R113, NH_3H_2O) was taken as 20°C.
- System performance is assumed to be stable and regular.
- Gravitational potential energy and kinetic energy are not taken into account.
- 1.compressor, 2. compressor, 1. pump and 2. pump met the energy they consumed from the turbines in their own systems.
- In the gas turbine, the inlet and outlet pressure ratio of the compressor is 21 and the temperature of the heat received from the heat source (HX1) is taken from the characteristics of the gas turbine 1493 K UGT-25000 [21]. 1/4 in 1st turbine
- 2.The turbine is reduced to atmospheric pressure. The power consumed by the 1st compressor is equal to the power produced by the 1st turbine. HX1 heat source 1800K.
- In the Rankine cycle, the 2nd heat exchanger temperature-dependent temperature transition is equalized. For the 3rd turbine and the 4th turbine, the maiden rise is 70°C, the pressure drop rates are 1.5.
- ORC 3.heat exchanger temperature-dependent heat transitions are equalized. The hard drop rates for the 5th turbine and the 6th turbine are 1.5.
- In the S-CO_2 evolution, the heat transitions due to the 4th heat exchanger temperature are equalized. 7.The pressure drop of the tube is 1.36 and the pressure drop of the 8th turbine is 1.46.
- In the absorption system, the generator was taken at 115°C. "Qu=quality (Saturated states, 0<=Qu<=1; Subcooled. Qu=-0.001; Superheated Qu=1.001)".
- Electricity ratio supplied to electrolyzer (0.5), HHV (141800), efficiency of the electrolyzer (0,56), Molecular mass(kJ/mol) H_2: 2.01594 , O_2: 31.9988 , H_2O: 18.01534, Standard chemical exergy(kJ/mol) H_2: 236.09 , H_2O: 0.9 , O_2: 3.97, [22].

B. ENERGY AND EXERGY ANALYZES

In thermodynamic analysis, an alternative formulation of the fundamental mass balance equation for steady-state conditions is as follows (1) [23,24-25];

$$\sum \dot{m}_{in} = \sum \dot{m}_{ex} \tag{1}$$

Expressing the mass flow rate as $\dot{m}$ and denoting the states at the inlet and outlet as 'in' and 'ex' respectively, the energy balance can be presented as follows (2):

$$\dot{Q}_{in} + \dot{W}_{in} + \sum_{in} \dot{m}\left(h + \frac{V^2}{2} + gz\right) = \dot{Q}_{ex} + \dot{W}_{ex} + \sum_{ex} \dot{m}\left(h + \frac{V^2}{2} + gz\right) \tag{2}$$

Here, $\dot{Q}$ is the heat transfer rate, , $\dot{W}$ is the power, h is the specific enthalpy, z is the height, v is the velocity and g is the gravitational acceleration. Steady-state conditions can be expressed alternatively through the entropy balance equation as (3):

$$\sum_{in} \dot{m}_{in} s_{in} + \sum_{k} \frac{\dot{Q}}{T_k} + \dot{S}_{gen} = \sum_{ex} \dot{m}_{ex} s_{ex} \tag{3}$$

Here, where s represents specific entropy and $\dot{S}_{gen}$ denotes the entropy generation rate, the exergy balance equation can be expressed as (4):

$$\begin{aligned} &\sum \dot{m}_{in}\, ex_{in} + \sum \dot{E}\, x_{Q,in} + \sum \dot{E}x_{W,in} \\ &= \sum \dot{m}0_{ex} ex_{ex} + \sum \dot{E}x_{Q,ex} + \sum \dot{E}x_{W,ex} + \dot{E}x_D \end{aligned} \tag{4}$$

The specific flow exergy can be written as (5):

$$ex = x_{ph} + ex_{ch} + ex_{pt} + ex_{kn} \quad (5)$$

The assumption of negligible contributions from kinetic and potential exergy components, as well as the neglect of chemical exergy, is made. The definition of physical or flow exergy (ex_{ph}) is provided in equation (6):

$$ex_{ph} = (h - h_o) - T_o(s - s_o) \quad (6)$$

In the context of the actual scenario, h and s stand for specific enthalpy and entropy, respectively. Meanwhile, h_o and s_o correspond to enthalpy and entropy at reference medium states.

Exergy destruction is equal to specific exergy times mass (7);

$$\dot{E}x_D = ex * m \quad (7)$$

$\dot{E}x_D$, are work-related exergy ratios and are given as (8):

$$\dot{E}x_D = T_0 \dot{S}_{gen} \quad (8)$$

$\dot{E}x_W$, are work-related exergy ratios and are given as (9):

$$\dot{E}x_W = \dot{W} \quad (9)$$

The exergy rates associated with heat transfer, denoted as $\dot{E}x_Q$, are presented in the following manner according to equation (10).

$$\dot{E}x_Q = \left(1 - \frac{T_o}{T}\right) \dot{Q} \quad (10)$$

Exergy destruction in the system (11);

$$\dot{E}x_{D,syst.} = \dot{E}x_{in} - \dot{E}x_{aut} \quad (11)$$

What work comes out of the system (12);

$$\dot{W}net_{out} = \dot{Q}_{in} - \dot{Q}_{out} \quad (12)$$

System thermal efficiency (η) (13)[26];

$$\eta = \frac{energy\ in\ exit}{total\ energy\ inlets} \quad (13)$$

The exergy efficiency (ψ) can be defined as follows;

$$\psi = \frac{exergy\ in\ exit}{total\ exergy\ inlets} \quad (14)$$

The electrolyzer analysisin the study shows the high heat value (HHV), Electricity ratio supplied to electrolyzer (η_{rat}),the efficiency of the electrolyzer (η_{elec}) and the hydrogen mass flow rate ($\dot{m}_{H2}$) (15):

$$\dot{m}_{H2} = (\eta_{elect} * \dot{W}net_{S-CO2} * \eta_{rat}) / HHV_{H2} \quad (15)$$

The chemical exergy of H_2, O_2 and H_2O can be obtained by:

$ex_{ch,H2}$=(236.09*1000)/MH_2
$ex_{ch,O2}$=(3.97*1000)/MO_2
$ex_{ch,H2O}$=(0.9*1000)/MH_2O

General energy equation (16);

$$\eta_{Total} = \frac{(\dot{W}_{t1}+\dot{W}_{t2})_{BC}+(\dot{W}_{t3}+\dot{W}_{t4})_{RC}+(\dot{W}_{t5}+\dot{W}_{t6})_{ORC}+(\dot{W}_{t7}+\dot{W}_{t8})_{S-CO2}+\dot{Q}^{AB}_{Cooling}+\dot{m}_{H2}LHV_{H_2}}{HX1+\dot{W}_{c1}+\dot{W}_{p1}+\dot{W}_{p2}+\dot{W}_{c2}+\dot{W}_{p3}+\dot{W}_{Elektrolyzer}} \quad (16)$$

General exergy equation (17);

$$\psi_{total} = \frac{\dot{E}x^{BC}_{\dot{W}_{t1}} + \dot{E}x^{BC}_{\dot{W}_{t2}} + \dot{E}x^{RC}_{\dot{W}_{t3}} + \dot{E}x^{RC}_{\dot{W}_{t4}} + \dot{E}x^{ORC}_{\dot{W}_{t5}} + \dot{E}x^{ORC}_{\dot{W}_{t6}} + \dot{E}x^{S-CO2}_{\dot{W}_{t7}} + \dot{E}x^{S-CO2}_{\dot{W}_{t8}} + \dot{E}x^{AB}_{Cooling} + \dot{m}_{H2}(ex^{ph}_{H_2} + \dot{m}_{29}ex^{ch}_{H_2})}{\dot{E}x^{Q}_{HX1} + \dot{E}x^{BC}_{\dot{W}_{c1}} + \dot{E}x^{RC}_{\dot{W}_{P1}} + \dot{E}x^{ORC}_{\dot{W}_{p2}} + \dot{E}x^{S-CO2}_{\dot{W}_{c2}} + \dot{E}x^{Abs}_{\dot{W}_{p3}} + \dot{E}x_{Elektrolyzer}} \quad (17)$$

In Table 1, the energy efficiency and exergy efficiency equations for each cycle are given separately.

Table 1. *Equations of energy efficiency and exergy efficiency of components in the integrated power cycle*

Cycle	Energy efficiency	Exergy efficiency
Air brayton cycle	$\frac{\dot{W}_{t1}+\dot{W}_{t2}}{HX1+\dot{W}_{c1}}$	$\frac{\dot{E}x^{BC}_{\dot{W}_{t1}}+\dot{E}x^{BC}_{\dot{W}_{t2}}}{\dot{E}x^{Q}_{HX1}+\dot{E}x^{BC}_{\dot{W}_{c1}}}$
H_2O rankine cycle	$\frac{\dot{W}_{t3}+\dot{W}_{t4}}{HX2+\dot{W}_{p1}}$	$\frac{\dot{E}x^{RC}_{\dot{W}_{t3}}+\dot{E}x^{RC}_{\dot{W}_{t4}}}{\dot{E}x^{Q}_{HX2}+\dot{E}x^{RC}_{\dot{W}_{P1}}}$
R113 ORC	$\frac{\dot{W}_{t5}+\dot{W}_{t6}}{HX3+\dot{W}_{p2}}$	$\frac{\dot{E}x^{ORC}_{\dot{W}_{t5}}+\dot{E}x^{ORC}_{\dot{W}_{t6}}}{\dot{E}x^{Q}_{HX3}+\dot{E}x^{RC}_{\dot{W}_{P2}}}$
S-CO_2 cycle	$\frac{\dot{W}_{t7}+\dot{W}_{t8}}{HX4+\dot{W}_{c2}}$	$\frac{\dot{E}x^{S-CO2}_{\dot{W}_{t7}}+\dot{E}x^{S-CO2}_{\dot{W}_{t8}}}{\dot{E}x^{Q}_{HX4}+\dot{E}x^{S-CO2}_{\dot{W}_{c2}}}$
Electolyzer	$\frac{\dot{m}_{H2}*HHV}{\dot{W}^{Net}_{S-CO2}}$	$\frac{\dot{m}_{H2}(ex^{ph}_{H_2}+\dot{m}_{29}ex^{ch}_{H_2})}{\dot{E}x_{Elektrolyzer}}$
NH_3H_2O Absorption cycle	$\frac{\dot{Q}^{HX7}_{Cooling}}{HX6+\dot{W}_{p3}}$	$\frac{\dot{E}x^{AB}_{\dot{W}_{t5}}+\dot{E}x^{AB}_{\dot{W}_{t6}}}{\dot{E}x^{Q}_{HX6}+\dot{E}x^{AB}_{\dot{W}_{P3}}}$

III. RESULTS AND DISCUSSION

The temperature entropy T-s diagrams of the integrated cycles are shown in figure 2(Rankine cycle), figure 3(ORC), and figure 4(S-CO_2 cycle).

Thermodynamic values of the state points of the air brayton cycle cycle in the integrated system in figure 1 are given in table 2.

***Table 2**. Thermodynamic values for the air brayton cycle*

Location	T[K]	$\dot{s}[\frac{kJ}{kg.K}]$	P[bar]	$\dot{h}[\frac{kJ}{kg}]$	$\dot{ex}[\frac{kJ}{kg}]$	$\dot{m}[\frac{kg}{s}]$	Fluid
1.	293.2	6.8446	1	293.4	0	88	air
2.	729.6	6.909	21	746	433.8	88	air
3.	1493	7.733	21	1630	1076	88	air
4.	1113	7.783	5.25	1177	609.1	88	air
5.	768	7.841	1	787.3	202.1	88	air
6.	512.3	7.412	1	516	56.56	88	air
7.	402.3	7.165	1	403.5	16.52	88	air
T[0].	293.2	6.846	1	293.4	--------	--------	air

T-s diagram for gradual H_2O Rankine cycle in figure 2.

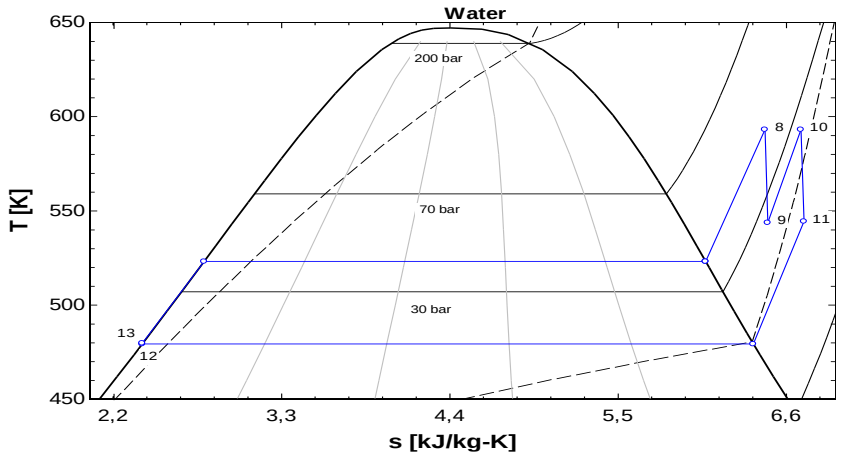

***Figure 2.** T-s diagram for H_2O Rankine cycle*

In table 3, thermodynamic values of the state points of the H_2O Rankine cycle in the integrated system in figure 2 are given.

***Table 3.** Thermodynamic values for the H_2O Rankine cycle*

Location	T[K]	$\dot{s}[\frac{kJ}{kg.K}]$	P[bar]	$\dot{h}[\frac{kJ}{kg}]$	$\dot{ex}[\frac{kJ}{kg}]$	$\dot{m}[\frac{kg}{s}]$	Fluid
8.	593.2	6.461	39.8	3017	1126	10.58	water
9.	543.8	6.478	26.53	2930	1034	10.58	water
10.	593.2	6.695	17.69	3053	1093	10.58	water
11.	544.4	6.715	17.69	2964	998.4	10.58	water
12.	479.4	2.389	39.8	880.5	182.9	10.58	water
13.	479.8	2.39	39.8	883.4	185.6	10.58	water
T[0].	293.2	0.2972	1	84.22	--------	--------	water

R113 T-s diagram for gradual ORC in figure 3

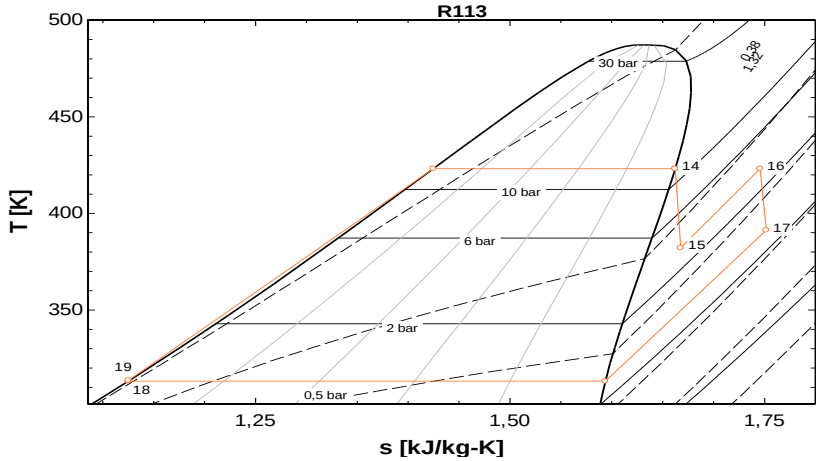

Figure 3. *R113 T-s diagram for ORC*

In table 4, thermodynamic values of the state points of the R113 ORC in the integrated system in figure 3 are given.

Table 4. *Thermodynamic values for the R113 ORC*

Location	T[K]	$\dot{s}[\frac{kJ}{kg.K}]$	P[bar]	$\dot{h}[\frac{kJ}{kg}]$	$\dot{ex}[\frac{kJ}{kg}]$	$\dot{m}[\frac{kg}{s}]$	Fluid
14.	423.2	1.662	12.22	448	54.26	63.92	R113
15.	408.9	1.664	8.146	442.6	48.49	63.92	R113
16.	423.2	1.692	8.146	454.5	51.99	63.92	R113
17.	411.5	1.694	5.431	448.6	45.62	63.92	R113
18.	382.7	1.319	5.431	425.8	39.65	63.92	R113
19.	383.2	1.319	12.22	305	11.79	63.92	R113
T[0].	293.2	1.064	1	218.3	--------	--------	R113

T-s diagram for gradual S-CO_2 cycle in figure 4.

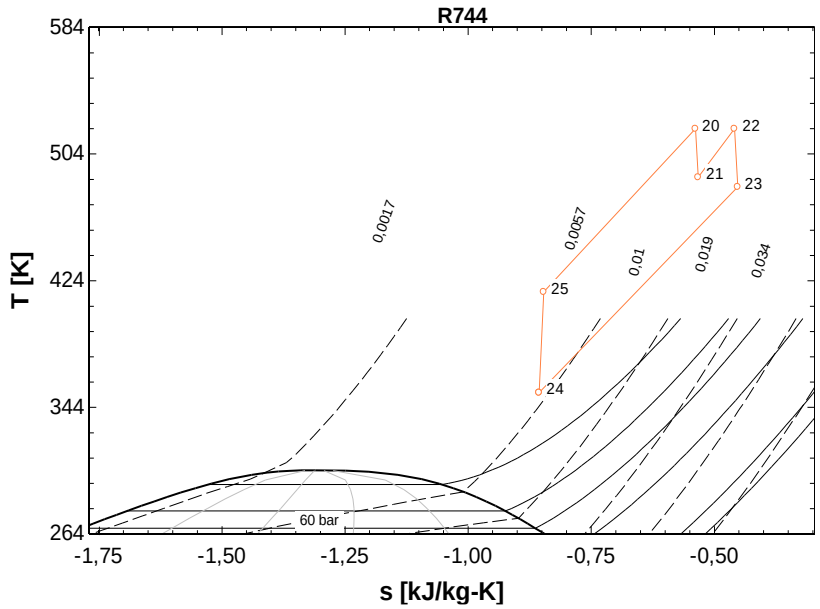

Figure 4. *T-s diagram for S-CO_2 cycle*

In table 5, thermodynamic values of the state points of the S-CO_2 cycle In the integrated system in figure 4 are given.

Table 5. *Thermodynamic values for the S-CO_2 cycle*

Location	T[K]	$\dot{s}[\frac{kJ}{kg.K}]$	P[bar]	$\dot{h}[\frac{kJ}{kg}]$	$\dot{ex}[\frac{kJ}{kg}]$	$\dot{m}[\frac{kg}{s}]$	Fluid
20.	520	-0.5385	180	158.5	317.4	122.4	CO_2
21.	489.4	-0.533	132	134.1	291.4	122.4	CO_2
22.	520	-0.4594	132	171.3	307	122.4	CO_2
23.	483.3	-0.4524	90	140.9	274.6	122.4	CO_2
24.	353.2	-0.8561	90	-25.11	226.9	122.4	CO_2
25.	416.9	-0.8463	180	15.51	264.7	122.4	CO_2
T[0].	293.2	-0.01403	1	-5.168	--------	--------	CO_2

In table 6, thermodynamic values of the state points of the Electolyzer in the integrated system in figure 1 are given.

Table 6. *Thermodynamic values for the Electolyzer*

Location	T[K]	$\dot{s}[\frac{kJ}{kg.K}]$	P[bar]	$\dot{h}[\frac{kJ}{kg}]$	$\dot{ex}[\frac{kJ}{kg}]$	$\dot{exch}[\frac{kJ}{kg}]$	$\dot{m}[\frac{kg}{s}]$	Fluid
44.	333.2	6.513	1	32.15	1.749	124.1	0.02695	O_2
45.	333.2	66.41	1	503.2	27.35	117112	0.003396	H_2
46.	298.2	0.3679	1	105.1	0	49.96	0.03035	H_2O
T[0].	298.2	0.7172	1	64.82	--------	--------	--------	H_2
T[0].	298.2	0.04569	1	6.411	--------	--------	--------	O_2

In table 7, thermodynamic values of the state points of the NH_3H_2O absorption cyclein the integrated system in figure 1 are given.

Table 7. *Thermodynamic values for the NH_3H_2O absorption cycle*

Location	T[K]	$\dot{h}[\frac{kJ}{kg}]$	$\dot{s}[\frac{kJ}{kg.K}]$	P [bar]	$\dot{ex}[\frac{kJ}{kg}]$	Qu [quality]	$\dot{m}$ [kg/s]	X [%NH3]	Fluid
26.	363.1	174.1	1.122	15	35.19	-0.001	32.126	0.400	NH_3H_2O
27.	388.2	1593.4	5.017	15	312.5	1	3.873	0.92	NH_3H_2O
28.	388.2	305.8	1.446	15	71.75	0	28.253	0.329	NH_3H_2O
29.	301.2	73.9	0.452	15	131.3	-0.001	3.873	0.920	NH_3H_2O
30.	255.1	73.9	0.524	1.9	110.1	0.162	3.873	0.920	NH_3H_2O
31.	275.2	1009.8	4.124	1.9	-9.33	0.812	3.873	0.920	NH_3H_2O
32.	301.2	-99.9	0.301	1.9	1.909	0.002	32.126	0.400	NH_3H_2O
33.	306.2	-80	0.3612	15	4.079	-0.001	32.126	0.400	NH_3H_2O
34.	323.5	16.9	0.633	15	21.29	-0.001	28.253	0.329	NH_3H_2O
35.	316.2	16.9	0.6385	1.9	19.64	0.01937	28.253	0.329	NH_3H_2O
T[0].	293.2	-8.949	0.6173	1	--------	--------	--------	--------	NH_3H_2O

The thermodynamic analysis of the combined power system created with different thermodynamic cycles is presented in Table 8 [(+) entering the system (-) exiting the system]. Compressor1 operates with an input power of 39825 kW and has a high efficiency of 95.86%. The exergy loss is 1648 kW, which is a reasonable value in the system. HX1 has an exergy loss of 8580 kW and operates at 86.82% efficiency, playing a significant role with a heat transfer of ± 77777 kW. Turbine1 operates with an output power of 39825 kW at a high efficiency of 96.88%, with an exergy loss of only 1283 kW. Similarly, Turbine2 operates with an output power of 34314 kW at 95.83% efficiency and has an exergy loss of 1495 kW. HX2 has an exergy loss of 2237 kW, operates at 72.71% efficiency, and handles a heat transfer of ± 23873 kW. HX3 has an exergy loss of 584.9 kW, operates at 70.71% efficiency, and handles a heat transfer of ± 9899 kW. Turbine3 operates with an output power of 916.2 kW at 94.33%

efficiency and has an exergy loss of 55.07 kW. Turbine4, similarly, operates with an output power of 942.1 kW at 93.92% efficiency and has an exergy loss of 61.01 kW. HX4 operates with an exergy loss of 951.1 kW at 88.98% efficiency and handles a heat transfer of ± 22045 kW. Pump1 operates with an input power of 30.29 kW at 93.89% efficiency and has an exergy loss of only 1.851 kW. Turbine5 operates with an output power of 341.8 kW at 92.62% efficiency and has an exergy loss of 27.25 kW. Turbine6 operates with an output power of 375.1 kW at 92.13% efficiency and has an exergy loss of 32.04 kW. HX5 has an exergy loss of 1617 kW, operates at 72.3% efficiency, and handles a heat transfer of ± 20325 kW. HX6 has an exergy loss of 88.73 kW, operates at 95.96% efficiency, and handles a heat transfer of ± 9218 kW. Pump2 operates with an input power of 35.92 kW at 92.35% efficiency and has an exergy loss of 2.749 kW. Turbine7 operates with an output power of 2980 kW at 93.75% efficiency and has an exergy loss of 198.8 kW. Turbine8 operates with an output power of 3712 kW at 93.67% efficiency and has an exergy loss of 250.9 kW. Compressor2 operates with an input power of 4971 kW at 92.95% efficiency and has an exergy loss of 350.6 kW. HX7 has an exergy loss of 118.7 kW, operates at 85.53% efficiency, and handles a heat transfer of ± 5885.7 kW. V1 has an exergy loss of 82.03 kW and operates at 83.87% efficiency. HX8 has an exergy loss of 78.29 kW, operates at 83.07% efficiency, and handles a heat transfer of ± 3625.2 kW. Pump3 operates with an input power of 640.2 kW at 10.89% efficiency and has an exergy loss of 570.5 kW. HX9 has an exergy loss of 426.1 kW, operates at 70.10% efficiency, and handles a heat transfer of ± 8162 kW. V2 has an exergy loss of 46.61 kW and operates at 92.24% efficiency. HX10 has an exergy loss of 225.2 kW, operates at 50.79% efficiency, and handles a heat transfer of ± 7597.7 kW. The electrolyzer operates with an input power of 1720 kW at 56% efficiency and has an exergy loss of 756.8 kW. The power output from the electrolyzer is 756.8 kW, operating at 78.35% efficiency, and has an exergy loss of 163.8 kW. Overall, most components in the system operate with high efficiency and maintain low exergy losses, which enhances the overall energy and exergy efficiency of the system.

Table 8. *Thermodynamic analysis of the combined power system*

Component	**W kW** (+) in (-) out	**$Ex_{D.}$ kW**	**φ[%]**	**Qheat** (+) in (-) out	**$\delta_{iz.}$[%]**
Compressor1 (1-2)	+39825	1648	95.86	--------	90
HX1 (2-3)	--------	8580	86.82	± 77777	--------
Türbine1 (3-4)	-39825	1283	96.88	--------	89.31
Türbine2 (4-5)	-34314	1495	95.83	--------	90
HX2 (5-6)(9-10)(8-13)	--------	2237	72.71	± 23873	--------
HX3 (6-7)(14-19)(15-16)	--------	584.9	70.71	± 9899	--------
Türbine3 (8-9)	-916.2	55.07	94.33	--------	90
Türbine4 (10-11)	-942.1	61.01	93.92	--------	89,31
HX4 (11-12)(21-22)(20-25)	--------	951.1	88.98	± 22045	--------
Pump1 (12-13)	+30.29	1.851	93.89	--------	90
Türbine5 (14-15)	-341.8	27.25	92.62	--------	90
Türbine6 (16-17)	-375.1	32.04	92.13	--------	89,31
HX5 (23-24)(42-43)	--------	1617	72.3	± 20325	--------
HX6 (17-18)(26-27-28)	--------	88.73	95.96	± 9218	--------
Pump2 (18-19)	+35.92	2.749	92.35	--------	90
Türbine7 (20-21)	-2980	198.8	93.75	--------	90
Türbine8 (22-23)	-3712	250.9	93.67	--------	90
Compressor2 (24-25)	+4971	350.6	92.95	--------	90
HX7 (27-29)(40-41)	--------	118.7	85.53	± 5885.7	--------
V1(29-30)	--------	82.03	83.87	--------	--------
HX8 (30-31)(38-39)	--------	78.29	83.07	± 3625.2	--------
Pump3 (32-33)	+640.2	570.5	10.89	--------	--------
HX9 (26-33)(28-34)	--------	426.1	70.10	± 8162	--------
V2 (34-35)	--------	46.61	92.24	--------	--------
HX10 (35-36-37)	--------	225.2	50.79	± 7597.7	--------

ELECTROLYZER					
Elektolyzere giren güç	+1720	756.8	56	--------	--------
ELECTROLYZER	+756.8	163.8	78.35	--------	--------

Table 9 shows the products coming out of one component. The Brayton cycle generates a net power output of 34,314 kW. The Rankine cycle produces a net power output of 1,828 kW. The Organic Rankine Cycle (ORC) generates a net power output of 681 kW. The cooling load handled by the system is 2,985 kW. The supercritical CO_2 (S-CO_2) cycle produces a net power output of 1,720 kW. Additionally, the system generates hydrogen at a rate of 0.0034 kg/s. Overall, these values highlight the contributions of each cycle to the integrated power system, demonstrating their roles in power generation, cooling, and hydrogen production.

Table 9. Net power values from integrated cycles

Parameters	Net Values
$\dot{W}_{BC}$	34314 kW
$\dot{W}_{RC}$	1828 kW
$\dot{W}_{ORC}$	681 kW
$\dot{Q}_{Cooling}$	2985 kW
$\dot{W}_{S-CO2}$	1720 kW
$\dot{m}_{Hydrogen}$	0.0034 kg/s

Table 10 shows the energy and exergy efficiency percentages of each component. The air Brayton cycle (BC) has an energy efficiency of 63% and an exergy efficiency of 27%. The H_2O Rankine cycle (RC) has an energy efficiency of 8% and an exergy efficiency of 5%. The R113 Organic Rankine Cycle (ORC) has an energy efficiency of 7% and an exergy efficiency of 10%. The supercritical CO_2 (S-CO_2) cycle has an energy efficiency of 25% and an exergy efficiency of 35%. The electrolyzer has an energy efficiency of 56% and an exergy efficiency of 70%. The NH_3H_2O absorption cycle has an energy efficiency of 36% and an exergy efficiency of 11%. For the total system, the combined energy efficiency is 66.35%, and the exergy efficiency is 35%. These values show the varying efficiencies of different cycles within the integrated power system, highlighting the overall performance and potential areas for improvement in both energy and exergy terms.

***Table 10.** Energy and exergy efficiency of components in the integrated power cycle*

Cycle	Energy efficiency [%]	Exergy efficiency [%]
Air brayton cycle(BC)	63	27
H_2O rankine cycle(RC)	8	5
R113 ORC	7	10
S-CO_2 cycle	25	35
Electolyzer	56	70
NH_3H_2O Absorption cycle	36	11
Total system	66.35	35

In the study conducted by Cao and colleagues [20], they successfully recuperated waste heat through the integration of diverse subsystems, including a thermoelectric generator, LiBr-H_2O absorption refrigerator system, heat recovery steam generator, and a proton exchange membrane electrolyzer. This

integrated approach resulted in an impressive exergy efficiency of 43% and an energy efficiency of 62.2%. In contrast, our study focuses on the utilization of waste heat from a gas turbine, and the system is enhanced through gradual expansion processes. The thermodynamic analysis of an integrated power generation system includes heat transitions to the H_2O Rankine cycle, R113 ORC cycle, S-CO_2 cycle, electrolyzer, and NH_3H_2O absorption cycle, each with successive sub-cycles. Moreover, by implementing gradual expansion in the Air-Brayton, R113-ORC, H_2O-Rankine, and S-CO_2 cycles, the process of extracting additional energy from turbines is initiated. The overall energy efficiency of our multi-integrated system is calculated to be 66.35%, with an exergy efficiency of 35%. Our study aligns with literature works, supporting the notion that the increased energy efficiency of the total integrated system is attributed to the high efficiency of gas turbines.

IV. CONCLUSION

The availability of energy serves as a fundamental criterion in determining its sustainability. Our initiative to harness waste heat sources, in conjunction with multiple power generation systems and systems featuring gradual expansion, represents a critical domain warranting extensive energy and exergy analysis. Within these systems, the discernible energy and exergy losses incurred during the utilization of energies sourced from diverse power origins unveil the operational availability of system components. Hence, meticulous analysis during both the design and operation phases is imperative to mitigate these losses effectively. Energy and exergy analysis emerges as a pivotal tool throughout the design, operation, and maintenance stages of such systems.

In the integrated system under consideration, the comprehensive energy efficiency of the system notably benefits from enhancements in the Air Brayton cycle and the Electrolyzer, representing pivotal cycles that augment overall efficiency. Notably, significant exergy breakdowns are observed in the heat transitions of the Air Brayton cycle and the S-CO_2 cycle. The resulting net power outputs indicate efficient utilization, with hydrogen production from the Electrolyzer, and substantial outputs from various cycles, including the Air Brayton cycle, H_2O Rankine cycle, R113 ORC, NH_3H_2O Absorption cycle, and S-CO_2 cycle. The achievement of high total energy yield underscores the efficacy of leveraging waste energy sources optimally.

In conclusion, our integrated power system demonstrates a robust energy efficiency of 66.35% and an exergy efficiency of 35%. This efficiency is driven by high-performing cycles such as the Air Brayton cycle and the Electrolyzer, which play crucial roles in optimizing overall system performance. Notably, significant energy outputs are observed across various cycles, including the Air Brayton, H_2O Rankine, R113 ORC, $NH3H_2O$ Absorption, and S-CO_2 cycles, along with hydrogen production from the Electrolyzer. These results underscore the effective utilization of waste heat sources and highlight opportunities for further enhancing energy and exergy efficiencies. Moreover, our study emphasizes the importance of rigorous energy and exergy analyses in guiding the design, operation, and maintenance of integrated energy systems, thereby advancing sustainable energy production practices.

V. REFERENCES

[1] Mohammadi, K., Ellingwood, K., & Powell, K. (2020). A novel triple power cycle featuring a gas turbine cycle with supercritical carbon dioxide and organic Rankine cycles: Thermoeconomic analysis and optimization. Energy Conversion and Management, 220, 113123.

[2] Ran, P., Zhou, X., Wang, Y., Fan, Q., Xin, D., & Li, Z. (2023). Thermodynamic and exergetic analysis of a novel multi-generation system based on SOFC, micro-gas turbine, S-CO_2 and lithium bromide absorption refrigerator. Applied Thermal Engineering, 219, 119585.

[3] Khan, M. S., Mubeen, I., Jingyi, W., Zhang, Y., Zhu, G., & Yan, M. (2022). Development and performance assessment of a novel solar-assisted multigenerational system using high temperature phase change material. International Journal of Hydrogen Energy, 47(62), 26178-26197.

[4] Khani, N., Manesh, M. H. K., & Onishi, V. C. (2022). 6E analyses of a new solar energy-driven polygeneration system integrating CO_2 capture, organic Rankine cycle, and humidification-dehumidification desalination. Journal of Cleaner Production, 379, 134478.

[5] Peng, W., Chen, H., Liu, J., Zhao, X., & Xu, G. (2021). Techno-economic assessment of a conceptual waste-to-energy CHP system combining plasma gasification, SOFC, gas turbine and supercritical CO_2 cycle. Energy Conversion and Management, 245, 114622.

[6] Khosravi, N. (2017). Design and Analysis of a Novel Renewable Multi-Generation System through Energetic and Exergetic. Investigation (Master's thesis, Eastern Mediterranean University EMU-Doğu Akdeniz Üniversitesi (DAÜ)).

[7] Panahirad, B. (2017). Thermodynamic Analysis of a Multi-Generation Plant Driven by Pine Sawdust as Primary Fuel (Master's thesis, Eastern Mediterranean University EMU-Doğu Akdeniz Üniversitesi (DAÜ)).

[8] Zhang, T., & Zhao, H. (2022). Thermodynamic analysis of a new hybrid system combined heat and power integrated solid oxide fuel cell, gas turbine, Rankine steam cycle with compressed air energy storage. Energy, 2004, 2965.

[9] Hai, T., Zhou, J., Almojil, S. F., Almohana, A. I., Alali, A. F., Mehrez, S., ... & Almoalimi, K. T. (2023). Deep learning optimization and techno-environmental analysis of a solar-driven multigeneration system for producing sustainable hydrogen and electricity: A case study of San Francisco. International Journal of Hydrogen Energy, 48(6), 2055-2074.

[10] Wu, B., Luo, Y., Feng, Y., Zhu, C., & Yang, P. (2023). Design and thermodynamic analysis of solid oxide fuel cells–internal combustion engine combined cycle system based on Two-Stage waste heat preheating and EGR. Fuel, 342, 127817.

[11] Qin, L., Xie, G., Ma, Y., & Li, S. (2023). Thermodynamic analysis and multi-objective optimization of a waste heat recovery system with a combined supercritical/transcritical CO2 cycle. Energy, 265, 126332.

[12] Atif, M., & Al-Sulaiman, F. A. (2017). Energy and exergy analyses of solar tower power plant driven supercritical carbon dioxide recompression cycles for six different locations. Renewable and Sustainable Energy Reviews, 68, 153-167.

[13] Elbir, A., Şahin, M. E., Özgür, A. E., & Bayrakçı, H. C. (2023). Thermodynamıc Analysıs Of A Novel Combıned Supercrıtıcal CO_2 And Organıc Rankıne Cycle. International Journal of Engineering and Innovative Research, 5(1), 33-47.

[14] Gogoi, T. K., Lahon, D., & Nondy, J. (2023). Energy, exergy and exergoeconomic (3E) analyses of an organic Rankine cycle integrated combined cycle power plant. Thermal Science and Engineering Progress, 41, 101849.

[15] Bamisile, O., Cai, D., Adedeji, M., Dagbasi, M., Hu, Y., & Huang, Q. (2023). Environmental impact and thermodynamic comparative optimization of CO_2-based multi-energy systems powered with geothermal energy. Science of The Total Environment, 168459.

[16] Elmaihy, A., Rashad, A., Elweteedy, A., & Nessim, W. (2023). Energy and exergy analyses for organic Rankine cycle driven by cooling water of passenger car engine using sixteen working fluids. Energy Conversion and Management: X, 20, 100415.

[17] Manesh, M. K., Mehrabian, M. J., Nourpour, M., & Onishi, V. C. (2023). Risk and 4E analyses and optimization of a novel solar-natural gas-driven polygeneration system based on Integration of Gas Turbine–SCO_2–ORC-solar PV-PEM electrolyzer. Energy, 263, 125777.

[18] Bamisile, O., Cai, D., Adedeji, M., Dagbasi, M., Li, J., Hu, Y., & Huang, Q. (2023). Thermo-enviro-exergoeconomic analysis and multi-objective optimization of a novel geothermal-solar-wind micro-multi-energy system for cleaner energy production. Process Safety and Environmental Protection, 170, 157-175.

[19] Ding, G. C., Peng, J. I., & Mei-Yun, G. E. N. G. (2023). Technical assessment of Multi-generation energy system driven by integrated renewable energy Sources: Energetic, exergetic and optimization approaches. Fuel, 331, 125689.

[20] Cao, Y., Habibi, H., Zoghi, M., & Raise, A. (2021). Waste heat recovery of a combined regenerative gas turbine-recompression supercritical CO_2 Brayton cycle driven by a hybrid solar-biomass heat source for multi-generation purpose: 4E analysis and parametric study. Energy, 236, 121432.

[21] Шкляр, В. И., Дубровская, В. В., Задвернюк, В. В., & Колпаков, А. Г. (2010). Эксергетический анализ работы газотурбинной установки. Промышленная теплотехника

[22] Szargut, J. (2007). Egzergia: poradnik obliczania i stosowania. Wydawnictwo Politechniki Śląskiej.

[23] Cengel YA, Boles MA, Thermodynamics: an engineering approach. McGraw-Hill New York; 2011.

[24] Dincer I, Rosen MA: Exergy: energy, environment and sustainable development. Elsevier Science; 2012.

[25] Bejan A., Tsatsaronis G., Moran M. 1996, Thermal design and optimization. New York: Jonh Wiley and Sons

[26] Elbir, A., Bayrakçi, H. C., Özgür, A. E., Deniz, Ö. (2022). Experimental analysis of a transcritical heat pump system with CO_2 refrigerant. International Advanced Researches and Engineering Journal, 6(3), 186-193.

[27] Klein SA. Engineering Equation Solver(EES) 2020, F-Chart Software, Version 10.835-3D.